Electronic Supplementary Material (ESI) for RSC Chemical Biology.

Supplementary Table 1. Crystallization conditions

Protein construct	**Crystallization conditions**
BKVP1.30-299	10 % PEG 3350, 0.2 M NaI, 0.1 M Bis-Tris, pH 5.5
BKVP1.26-299	17 % PEG 3350, 65 mM tri-ammonium citrate, 0.1 M HEPES, pH 7.0
BKVP1.26-299.C104S	13 % PEG 3350, 0.3 M Na formate
BKVP1.Cfusionlong (containing C-terminal residues 315-335)	22 % ethylene glycol, 11 % PEG 8000, 50 mM sodium nitrate, 50 mM sodium phosphate dibasic, 50 mM ammonium sulfate, 0.1M imidazole, 0.1 M MES, pH 6.5
BKVP1.Cfusionshort (containing C-terminal residues 325-335)	18 % PEG 3350, 0.2 M NaCl, 0.1 M Tris, pH 8.5
JCVP1.18-291	10 % PEG 4000, 0.1 M HEPES, 0.1M MOPS, pH 7.1, 87 mM $MgCl_2$

Supplementary Table 2. X-ray data collection and refinement statistics

	BKVP1.30-299	**BKVP1.26-299.C104S**	**BKVP1.Cfusionlong**
PDB entry	7B6A	7B69	7B6C
Data collection			
Resolution range (Å)	50 - 1.44 (1.49 - 1.44)	99 – 1.47 (1.55 - 1.47)	90 - 2.48 (2.57 - 2.48)
Space group	$P2_12_12$	$P2_1$	$C2$
a, b, c (Å)	138.6, 149.7, 65.5	62.0, 135.7, 156.4	234.3, 97.2, 146.2
α, β, γ (°)	90, 90, 90	90, 95.0, 90	90, 98.4, 90
Unique reflections	245801 (24335)	418028 (51986)	113999 (11185)
Multiplicity	13.2 (11.8)	2.8 (1.5)	3.7 (3.8)
Completeness (%)	99.9 (99.8)	96.6 (82.6)	99.0 (98.2)
Mean I/σ(I)	16.4 (1.3)	9.2 (1.1)	6.3 (1.6)
R_{pim}	0.0293 (0.562)	0.047 (0.393)	0.111 (0.618)
$CC_{1/2}$	0.999 (0.62)	0.997 (0.695)	0.984 (0.60)
Refinement			
R_{work}	0.168	0.181	0.204
R_{free}	0.189	0.197	0.234
No. VP1 pentamers / ASU	1	2	2
No. of non-H atoms			
protein	10358	20680	21385
solvent	1523	1978	863
RMSD bonds (Å)/angles(°)	0.015/1.9	0.012/1.6	0.014/1.9
Ramachandran favoured/outliers (%)	96.5/0.5	96.5/0.4	96.1/0.4
Average B-factor (Å^2)	24.5	24.6	43.6
protein	22.7	22.1	43.8
solvent	35.9	28.7	38.3

Statistics for the highest-resolution shell are shown in parentheses

Supplementary Table 3. Effect of designed point mutations in VP1 on viral viability

Pocket	Virus	Mutation	Effect on viral viability	Reference
F50	SV40 ^	E48A*	10^5-fold decrease in virus titre	[1]
		E216K *	10^6-fold decrease in virus titre	
		E329A+E330A	10^6-fold decrease in virus titre	
		E330K	Non-viable mutant	
		E330R	10^8-fold decrease in virus titre	
		E329A+E330R E329A+E330K	Non-viable mutants	
R92	Hamster PyV	G336A #	Formation of aberrant particles	[2]
M109	SV40 ^	P300G	>10^7-fold decrease in virus titre (pfu/ml), 4-fold decrease in virus stability	[3]
		P300A	10^3-fold decrease in virus titre	
		Y299A	4-fold decrease in virus stability	
		Y299T	2-fold decrease in virus stability	
		L305P	No capsid assembly	[4]
		L308P		
		R311A	Formation of aberrant particles	
		F303A+L304F		
		D307A+R311A		
		L304W		

** These mutations were introduced in the core domain. All other mutations were introduced in the regions of the C-terminal arm interacting with the indicated pocket*

^ Residue numbering coincides with that of BKPyV VP1

 # Third residue of the highly conserved VDGQ sequence within the C-terminal arm. Corresponds to G318 of BKVP1

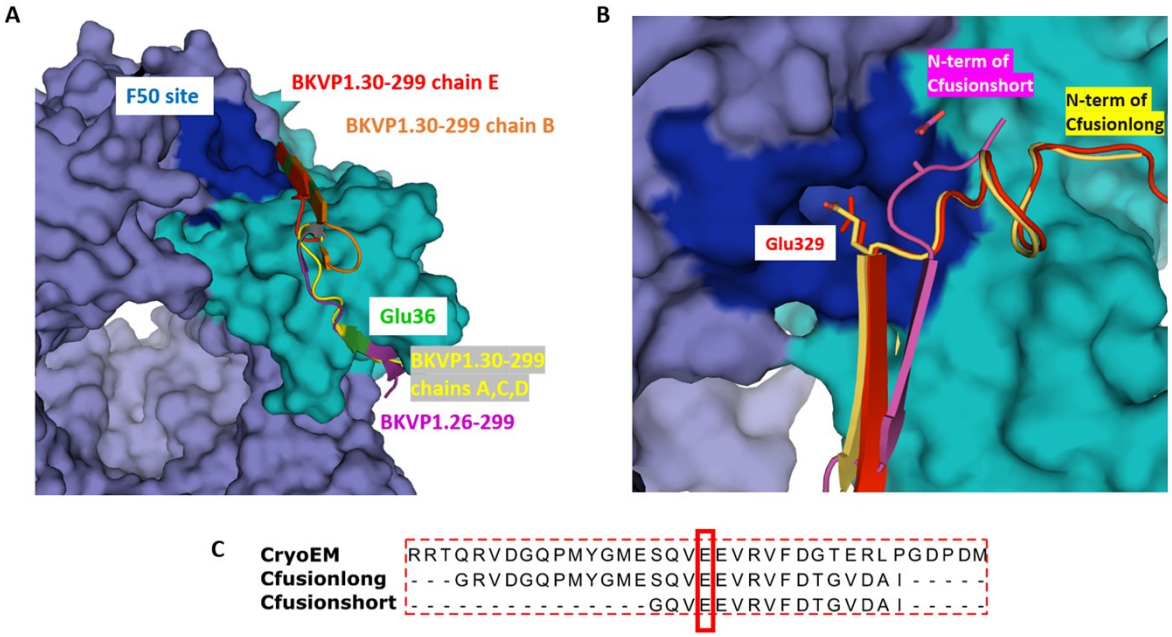

Supplementary Figure 1. Comparison of crystal structures. A. Varied conformation of the N-terminal region observed in the crystal structure of BKVP1.30-299. Five chains found in the asymmetric unit of the $P2_12_12$ crystal form are superimposed. The N-terminal regions (residues 30-39) are shown as ribbons in distinct colours, with the position of residue E36 highlighted in green. In chains B and E, this region is forming an extra β-strand which folds back on the first β-strand normally present in the core domain (residues 44 to 52). As a result, the right-hand side of the fragment-binding pocket F50 is altered. In the crystal structure of the BKVP1.26-299 construct, the N-terminal regions of all protein chains are located away from the F50 pocket. The conformation of the complete N-terminal arm (residues 1-39) in the crystal structure of full-length VP1 from SV40 [5] as well as in the cryoEM structure of BKVP1 [6] is again different (not shown), but also not interfering with the F50 pocket. **B.** Conformation of the C-terminal arm as seen in the crystal structures of Cfusionlong and Cfusionshort (this work) and the full-length cryoEM structure [6]. The structures were superimposed by the core pentamer (surface). Side chains of E329 are shown. **C.** Sequence alignment of residues 311 to 346 that patch an adjacent pentamer in the full-length cryoEM structure, with the N-terminal regions of BKVP1.Cfusionlong and BKVP1.Cfusionshort. The residue E329 is highlighted.

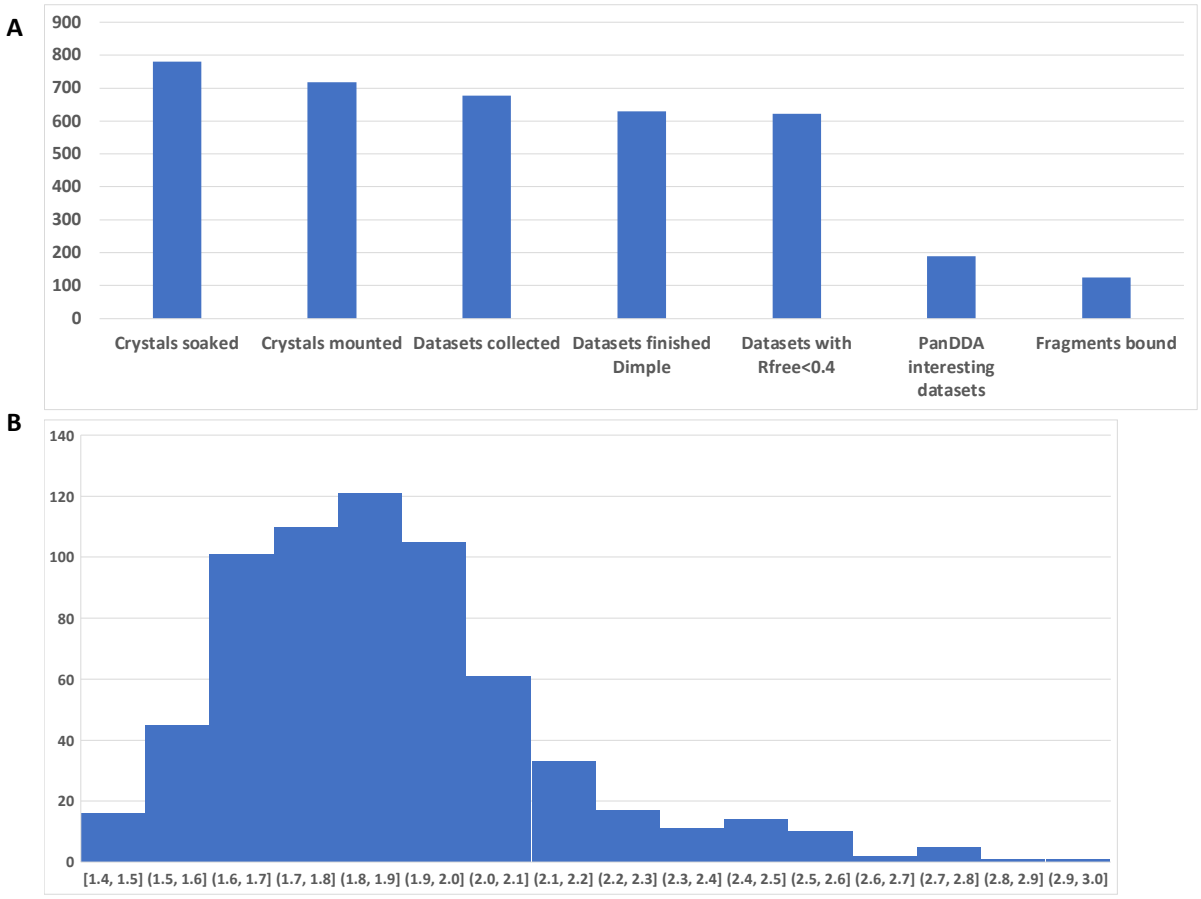

Supplementary Figure 2. Statistics of the main XChem fragment screening. A. Number of datasets retained on specific stage. **B.** Distribution of the resolution for the datasets collected from soaked crystals. High resolution cut-off was defined by $CC_{1/2}$=0.3 (Reference [7]).

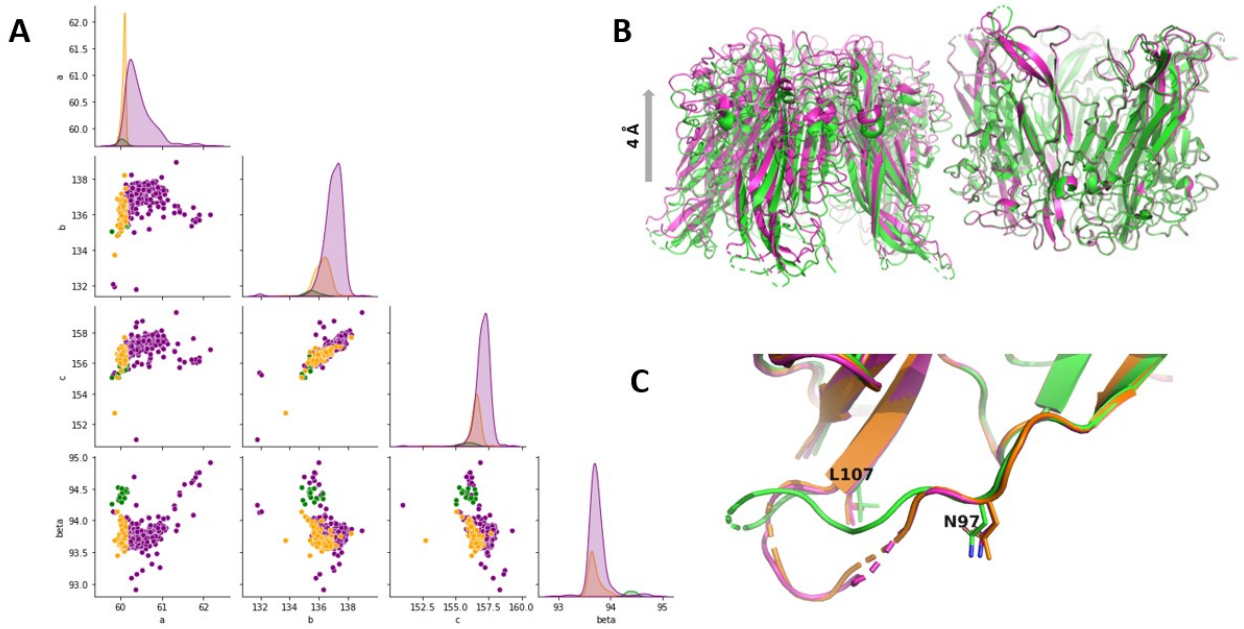

Supplementary Figure 3. Clustering analysis of datasets collected during the main XChem screening. Data for the three clusters established through PanDDA2 analysis are shown in magenta, orange and green respectively. **A.** Distributions (diagonal) and pairwise plots of the unit cell parameters *a,b,c* and *β*. The space group was $P2_1$. Plot produced with Seaborn. **B.** Ribbon diagrams of the two pentamers in the asymmetric unit for representative structures from the first (magenta) and the third (green) clusters aligned using rightmost pentamer. In the two clusters, the relative position of the left-side pentamer differs by 4Å. **C.** Conformation of the CD loop in chain I of representative structures of the three clusters. CD loop-flanking residues Asn97 and Leu 107 are depicted by sticks.

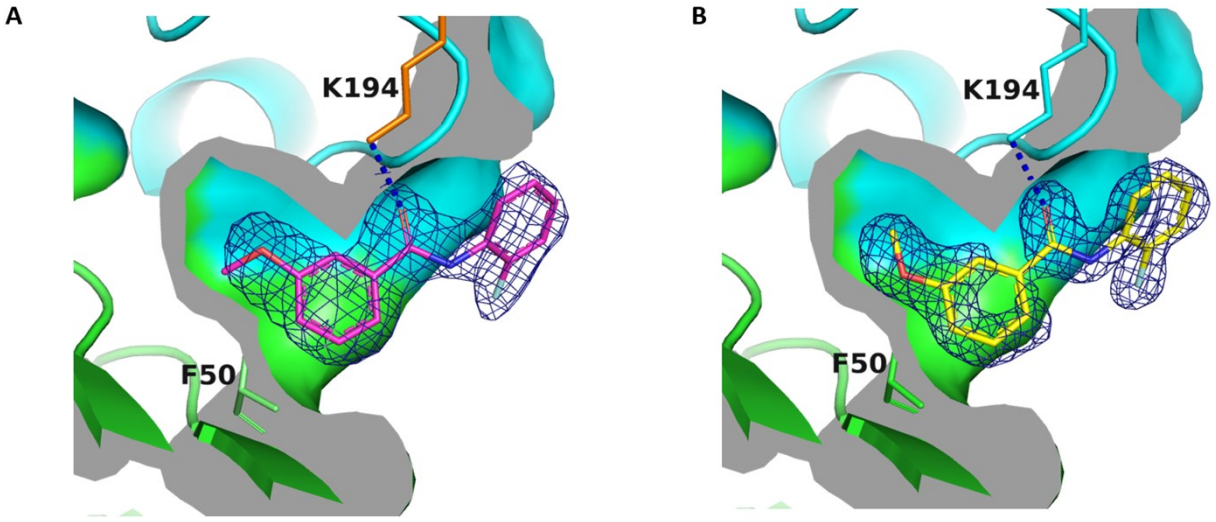

Supplementary Figure 4. Fragment placement in electron density. A. A drug-like fragment (N-(2-fluorophenyl)-3-methoxybenzamide) from the DSP library could be placed in the F50 pocket after the preliminary XChem screening. The resolution of the data was 2.3 Å. 2Fo-Fc electron density map at 1σ level is drawn. **B.** The same fragment is also part of the DSiP library. After the final XChem screening round, its pose could be refined thanks to the improved resolution (1.7 Å).

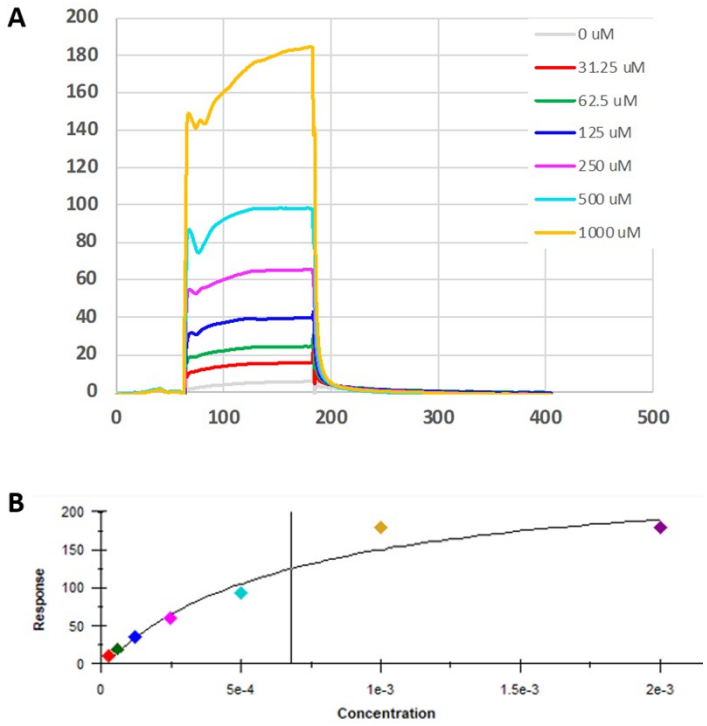

Supplementary Figure 5. SPR data for binding of TFP to the BKVP1.30-299 construct. A. Baseline-subtracted SPR curves obtained with increasing TFP concentrations. B. Resulting dose-response curve. Vertical line shows the estimated K_D value.

Supplementary references

1. Li, P. P. *et al.* Importance of Vp1 Calcium-Binding Residues in Assembly, Cell Entry, and Nuclear Entry of Simian Virus 40. *Journal of Virology* **77**, 7527–7538 (2003).

2. Gedvilaite, A., Aleksaite, E., Staniulis, J., Ulrich, R. & Sasnauskas, K. Size and position of truncations in the carboxy-terminal region of major capsid protein VP1 of hamster polyomavirus expressed in yeast determine its assembly capacity. *Archives of Virology* **151**, 1811–1825 (2006).

3. Ben-nun-Shaul, O., Bronfeld, H., Reshef, D., Schueler-Furman, O. & Oppenheim, A. The SV40 Capsid Is Stabilized by a Conserved Pentapeptide Hinge of the Major Capsid Protein VP1. *Journal of Molecular Biology* **386**, 1382–1391 (2009).

4. Yokoyama, N. *et al.* Mutational analysis of the carboxyl-terminal region of the SV40 major capsid protein VP1. *Journal of Biochemistry* **141**, 279–286 (2007).

5. Stehle, T., Gamblin, S. J., Yan, Y. & Harrison, S. C. The structure of simian virus 40 refined at 3.1 Å resolution. *Structure* **4**, 165–182 (1996).

6. Hurdiss, D. L., Frank, M., Snowden, J. S., Macdonald, A. & Ranson, N. A. The Structure of an Infectious Human Polyomavirus and Its Interactions with Cellular Receptors. *Structure* **26**, 839–847 (2018).

7. Beilsten-Edmands, J. *et al.* Scaling diffraction data in the DIALS software package: Algorithms and new approaches for multi-crystal scaling. *Acta Crystallographica Section D: Structural Biology* **76**, 385–399 (2020).